J Mater Sci (2020) 55:3064–3072

Metals & corrosion

Mechanism of intermetallic compound formation during the dissimilar friction stir welding of aluminum and steel

Tsutomu Tanaka[1,*], Masayuki Nezu[1], Sohei Uchida[1], and Tomotake Hirata[1]

[1] *Research Division of Metallic Materials, Osaka Research Institute of Industrial Science and Technology, 2-7-1 Ayumino, Izumi, Osaka 594-1157, Japan*

Received: 8 May 2019
Accepted: 30 September 2019
Published online: 10 October 2019

ABSTRACT

The formation of intermetallic compounds (IMCs) during the friction stir welding (FSW) of aluminum and steel is problematic because these IMCs can reduce weld strength. In this study, the mechanism behind the observed rapid growth of IMCs during the dissimilar FSW of aluminum and steel was investigated. The temperature during welding was measured using *K*-type thermocouples, and the microstructures of cross sections of the welded materials were examined via scanning electron microscopy. Microstructural observations indicated that the growth of IMCs was not constant, but occurred in two rapid growth steps. The first phase of rapid IMC growth was observed immediately after the probe contacted the steel, while the second began in the region subjected to the large downward pressure of the tool shoulder on the steel plate. The measurements showed that the temperature underneath the tool shoulder was higher than that at the tool probe. Additionally, it was found that the two IMC growth steps and the growth rate could be expressed by an equation based on metallic diffusion and the measured temperatures. As the IMCs grew rapidly via contact between the steel plate and the tool probe or shoulder, it is necessary to control such contacts to inhibit IMC growth. This strategy and the proposed formula for predicting IMC growth rates could help improve the strength of welds during the fabrication of lightweight materials in the automotive and aerospace industries.

Address correspondence to E-mail: t_tanaka@tri-osaka.jp

https://doi.org/10.1007/s10853-019-04106-2

Introduction

In the automotive industry, there are economic and environmental motivations to reduce the weight of vehicles, thus increasing their energy efficiency and reducing energy costs [1]. Replacing steel parts with lighter metals, such as aluminum and its alloys, is one of the major weight-saving techniques employed [2]. Hence, the joining of dissimilar materials (specifically, aluminum to steel) has been extensively investigated [3–9]. However, it is difficult to produce durable welds between aluminum and steel using conventional fusion welding, as the high heat input during this process results in the formation of large amounts of intermetallic compounds (IMCs) that can reduce the strength and durability of the weld. Therefore, a lower heat input is essential for producing a sound joint between aluminum and steel.

Friction stir welding (FSW) [10, 11] is a relatively new joining technique that can achieve high-quality welded joints; hence, it has been applied to various materials, including aluminum alloy [12–14], steel [15, 16], magnesium alloy [17, 18], titanium alloy [19, 20], and nickel-based alloy [21, 22]. Additionally, FSW has recently attracted major interest as a promising technique for joining aluminum to steel because it has several advantages over more standard techniques, such as a low heat input, short welding time, and superior mechanical properties of the weld [23–27]. Fukumoto et al. [28] reported that a dissimilar joint between cast aluminum alloy and mild steel had approximately the same strength as that of the aluminum base material, which was achieved by optimizing the offset of the pin periphery from the butt interface. Morita et al. [29] and Tanaka et al. [30] also reported that dissimilar FSW butt joints between aluminum alloys and steels exhibited good bending properties and excellent deep-drawing formability. However, abundant IMCs were formed and degraded mechanical properties were observed when the FSW conditions were not optimized. For example, Kimapong et al. [31] reported that the strength of an FSW joint with an IMC thickness of ~ 7 μm was ~ 60% lower than that with an IMC thickness below 1 μm. Moreover, Tanaka et al. [32] indicated that strength increased exponentially with a reduction in the IMC thickness, where the strengths of FSW joints with IMC thicknesses of ~ 1 μm and ~ 0.1 μm were approximately 100 MPa and 330 MPa, respectively. Therefore, it is necessary to inhibit IMC formation and elucidate the IMC growth mechanism during FSW in order to develop reliable and strong FSW joints between aluminum and steel.

Tanaka et al. [33] analyzed the IMC growth mechanism in FSW butt joints during static welding (i.e., wherein the tool was inserted into the plate, but not moved), which is a process similar to friction stir spot welding. Use of this method was necessary in order to maintain a constant temperature for a long enough period to investigate the IMC growth rate. In their study, it was shown that IMC growth was dominated by diffusion that was similar to diffusion bonding and roll bonding, where rapid IMC growth occurred for a brief period during the operation of the welding tool. However, this period of rapid IMC growth was not investigated in their study. As it is very important to clarify the IMC growth mechanism under actual FSW conditions, in this study, the rapid growth mechanism of IMCs during the operation of a welding tool was investigated by combining a previously proposed theoretical formula with experimental results from microstructural observations and analyses of welding temperature. Additionally, the predominant factors controlling IMC growth during FSW were considered.

Materials and methods

Sheets of mild steel and A1050 aluminum alloy, both with a thickness of 3 mm, were used in this study. Figure 1 presents diagrams of the dissimilar friction

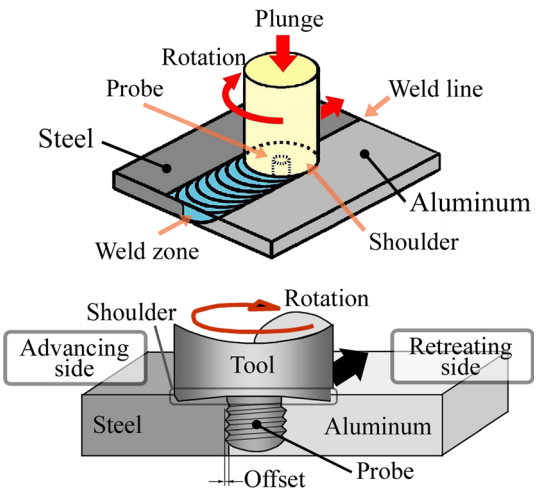

Figure 1 Diagrams of the dissimilar friction stir welding (FSW) process.

stir welding process; as is shown, the aluminum and mild steel plates were located on the retreating side and advancing side, respectively. The advancing side of the weld was the side on which the rotation of the tool proceeded in the same direction as the motion of the tool itself. The opposite side is referred to as the retreating side. Moreover, the probe center was offset from the butt interface so that the tool probe contacted the steel over a width of ~ 0.2 mm. Friction stir welding was performed at a tool rotation speed of 1800 rpm and a weld travel speed of 100 mm min^{-1}. An FSW tool with a screw thread probe made of SKD61 tool steel was used with a shoulder diameter of 12 mm, probe diameter of 4 mm, and probe length of 2.9 mm, as shown in Fig. 2.

The inclination angle during FSW was 3°, and temperatures were measured via *K*-type thermocouples at the tool probe (T_p) and tool shoulder (T_s) using a non-contact temperature measurement system (FSW-2000 Series telemetry system; Megastir, USA). Microstructural observations of the interface of the weld were performed on cross sections cut perpendicular to the welding direction (region A in Fig. 3) and perpendicular to the normal direction of the sheets (region B in Fig. 3) using field emission electron microprobe analysis (EMPA; JXA-8530F, JEOL Ltd., Japan). The thickness of the IMC layer at the joint interface was calculated as the mean of ten

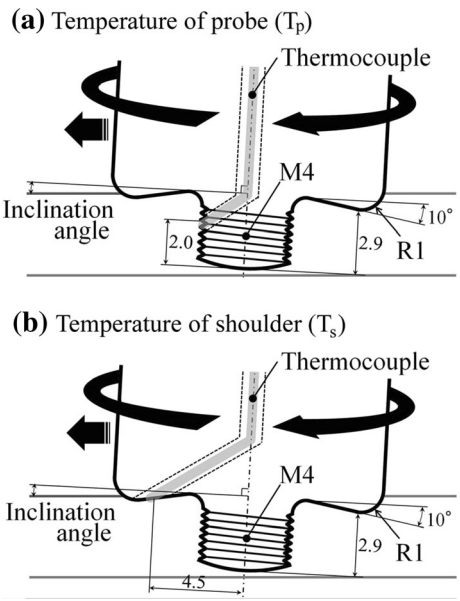

Figure 2 Diagrams of the method of measuring the welding temperature **a** of the probe (T_p) and **b** of the shoulder (T_s) using *K*-type thermocouples.

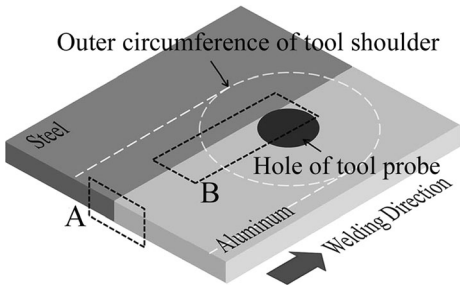

Figure 3 Schematic showing the regions of the welds observed using scanning electron microscopy (SEM).

IMC thicknesses randomly measured from scanning electron microscopy (SEM) images at 10000× magnification. In order to characterize the properties of the developed IMCs, transmission electron microscopy (TEM), bright-field imaging, and selected area electron diffraction (SAED) analyses were performed using a JEOL JEM-2000FX transmission electron microscope operated at 150 kV (Jeol Ltd., Japan). The TEM sample of the interface region was prepared using a focused ion beam (FIB; FB-2000, Hitachi High Technologies Inc., Japan).

Results and discussion

Microstructure and growth behavior of IMCs

A typical surface morphology of a weld is shown in Fig. 4a. The weld was successfully joined without

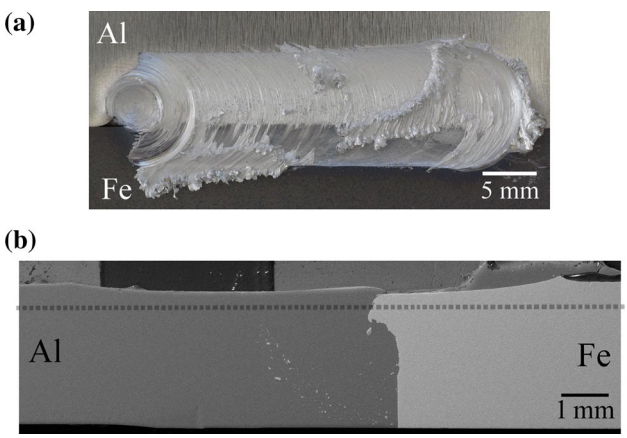

Figure 4 **a** Top surface view of the weld area and **b** typical SEM image showing the microstructure of the cross section perpendicular to the welding direction. The horizontal dashed line indicates the plane cut for observing the cross section perpendicular to the normal direction of the sheets.

obvious porosity or defects, though some splashes of material from the plate were observed. Figure 4b shows a micrograph of the cross section perpendicular to the welding direction (region A in Fig. 2), while fine fragments of the mild steel were distributed in the aluminum region and no voids or cracks were formed at the joint interface or in the weld zone.

Figure 5a shows a typical TEM image of the microstructure of the IMC. The IMC layer consisted of dual sub-layers denoted as Phase 1 (adjacent to the aluminum) and Phase 2 (adjacent to the iron). Phase 1 was composed of the equiaxed and fine grains with a grain size of less than 100 nm. Meanwhile, elongated grains with a layer thickness of ~ 300 nm were observed in Phase 2. Figure 5b and c shows a high-magnification TEM micrograph from the region near Phase 1 and the SAED pattern of grain A, respectively. Figure 5d and e shows a high-magnification TEM micrograph from the region near the Phase 2 and the SAED pattern of grain B, respectively.

The SAED analysis of the patterns shown in Fig. 6c and e confirmed $FeAl_3$ (Al-rich part) and Fe_2Al_5 structures (Fe-rich part), respectively. Ogura et al. [24], Tanaka et al. [34], and Sun et al. [35] reported the formation of an amorphous structure at the joint interface. However, similar to our results, Van der Rest et al. [36] and Movahedi et al. [37] reported that

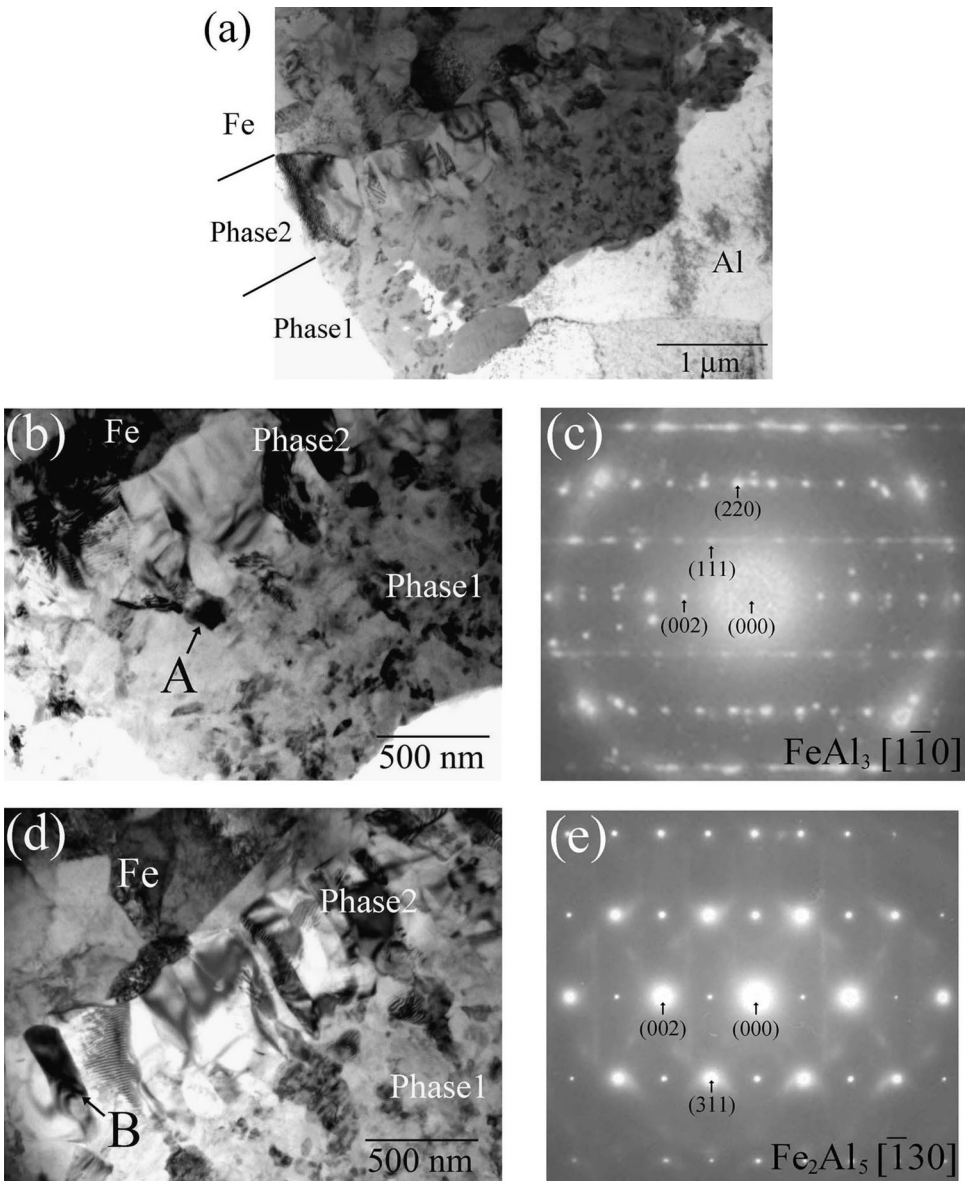

Figure 5 **a** Typical transmission electron microscopy (TEM) image at the joint interface, **b** high-magnification TEM micrograph near Phase 1, **c** the corresponding selected area electron diffraction (SAED) pattern for grain A, **d** high-magnification TEM micrograph near Phase 2, and **e** the corresponding SAED pattern for grain B.

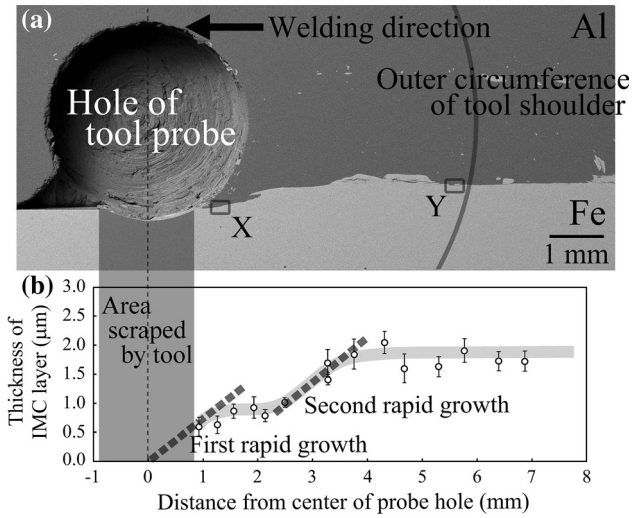

Figure 6 **a** Typical SEM image showing the microstructure of the cross section perpendicular to the normal direction of the sheets. **b** Intermetallic compound (IMC) thickness profile as a function of distance from the center of the probe hole.

the IMC was composed of two sub-layers of $FeAl_3$ and Fe_2Al_5. The microstructures and composition of the IMC at the interface thus depend on the heat input and degree of plastic deformation.

In this study, the tool rotation speed was higher than in previous studies in which the formation of an amorphous structure at the joint interface was reported [24, 34, 35]. Due to the higher heat input, no amorphous structure formed, but instead two IMCs formed at the joint interface. The existence of excessively thick IMC layers deteriorates joint properties; however, the IMC layer drives the metallurgical bonding of aluminum alloys and steels, resulting in a better weld quality [24, 38]. Although it is important to prevent IMC formation to improve joint properties, controlling IMC formation is difficult. Therefore, a method for controlling IMC growth during FSW was considered with respect to the IMC growth mechanism during FSW.

A micrograph of the cross section perpendicular to the normal direction of the sheets is shown in Fig. 6 and corresponds to region B in Fig. 2. The observed plane is shown by the dashed line in Fig. 4b. It was found that the welding line shifted toward the aluminum side after the tool probe contacted the steel (Fig. 6a). As shown in Fig. 3, the tool shoulder contacted and applied pressure to the steel plate during FSW due to the inclination angle of 3°. Therefore, the shift in the welding line indicates that the steel was plastically deformed by the tool shoulder pressure. Additionally, the effect of this pressure was found to be significant from a distance of ~ 2 mm from the center of the tool probe hole, as shown in Fig. 6a. Figure 7a and b shows high-magnification SEM images of the joint interface at distances of 1.7 and 5.8 mm from the center of the tool probe hole, respectively; these correspond to the observation positions *X* and *Y* shown in Fig. 6a. The mean IMC thicknesses shown in Fig. 7a and b are ~ 0.7 μm and 1.7 μm, respectively.

The relationship between the mean IMC thickness and standard deviation to the distance from the center of the tool probe is shown in Fig. 6b. Point 0 in Fig. 6b corresponds to the probe-hole center in Fig. 6a, where their distance scales are the same. It can be seen from Fig. 6b that IMC growth during FSW was not constant, but occurred in two rapid growth steps. First, IMC growth was observed immediately after the tool probe contacted the steel, and then growth was inhibited. Subsequently, a second rapid growth stage began 2.2 mm from the center of the probe hole, where plastic deformation of the steel under the pressure of the tool shoulder became significant (Fig. 6a). However, IMC growth was not observed over a distance of approximately

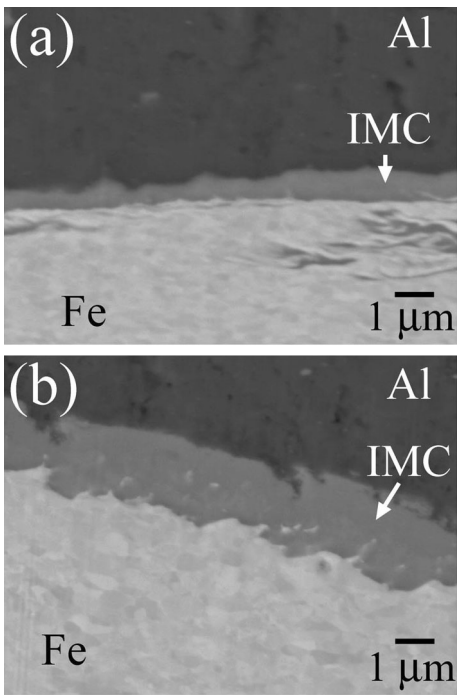

Figure 7 Scanning electron microscopy images (backscattered electron imaging mode) showing the microstructure of positions **a** *X* and **b** *Y*, as indicated in Fig. 5.

4.5 mm. As shown in Fig. 2, the tool used in this study had a curved 1 mm radius to the corner of the tool shoulder. Therefore, the lack of IMC growth is because the peripheral part of the tool was not subjected to the downward pressure of the tool shoulder on the steel plate due to the curvature relative to the tool corner. Additionally, the tool was extracted from the plates quickly after the tool arrived at the final location. The reduction in heat input was also expected to result in the reduction in the IMC growth rate. Consequently, the growth rate trend was consistent with the microstructural changes observed due to contact between the tool and steel plate.

Temperatures during FSW

It is well known that IMC thicknesses increase with increasing welding temperature. Thus, temperatures near the probe and underneath the tool shoulder (T_s and T_p, respectively) were measured in order to clarify the difference between the two rapid IMC growth processes. Figure 8 shows the two temperature profiles measured by *K*-type thermocouples. Both temperatures increased immediately after the welding tool came into contact with the plates, and remained nearly constant for ~ 6 s. Additionally, the temperatures were nearly unchanged while the tool was traveling along the weld. The T_s and T_p were approximately 780 K and 730 K, respectively. We interpret these results to mean that the temperature during the FSW of aluminum and steel is strongly influenced by contact between the tool and steel plate. As shown in Fig. 1, the tool probe contacted the side of the steel plate due to the tool offset, while the tool shoulder applied pressure to the surface of the steel plate predominantly due to the inclination angle (3°). Therefore, the different temperatures produced by these tool contacts appear to affect the IMC growth mechanism during FSW.

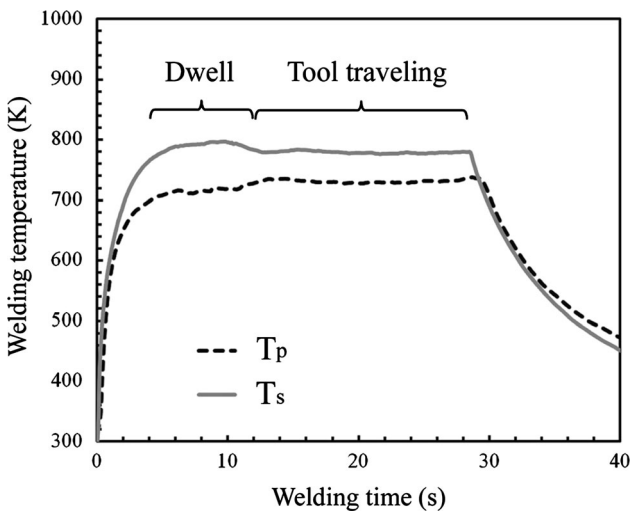

Figure 8 Thermal history of the tool probe and shoulder.

IMC growth process during FSW

There have been several studies in which the IMC layer growth kinetics of aluminum and steel have been analyzed [39–42]. However, the growth mechanisms of IMC layers are diffusion bonding and isothermal heating, which are also favorable for temperature measurements; yet, very little information is available on IMC growth kinetics during FSW due to the difficulty of measuring temperatures synchronously. Tanaka et al. [33] reported on the growth rate of an IMC during FSW. The two rapid IMC growth steps revealed by microstructural observations in this study were considered from a growth kinetics perspective, using the temperatures measured experimentally and the diffusion rate equation. Tanaka et al. [33] also reported that the growth rate of an IMC during FSW could be calculated using the following equation, based on metallic diffusion:

$$K = \frac{d^2}{t} = 9.6 \times 10^{-3} \exp\left(-\frac{144000}{RT}\right), \quad (1)$$

where K is the growth rate constant, d is the thickness of the IMC, t is the heating time, R is the universal gas constant [8.314 J/(mol. × K)], and T is the absolute temperature. The relationship between the mean IMC thickness and standard deviation to the welding time at temperatures of 730 K and 780 K was calculated using Eq. (1), and the results are shown in Fig. 9. The welding time was calculated based on the welding speed and distance from the center of the probe hole, while the IMC thicknesses measured from the SEM images are also plotted in this figure. As shown in Fig. 9, the experimental data for the first stage of rapid IMC growth agreed well with the calculated values for 730 K, which is the T_p in the region of 2 mm from the center of the probe hole. This indicates that the first rapid stage of growth was strongly influenced by contact with the tool probe.

In the region from 1.3 s (location of measured T_p) to 2.8 s (location of measured T_s), the temperature was expected to gradually increase from 730 to 780 K;

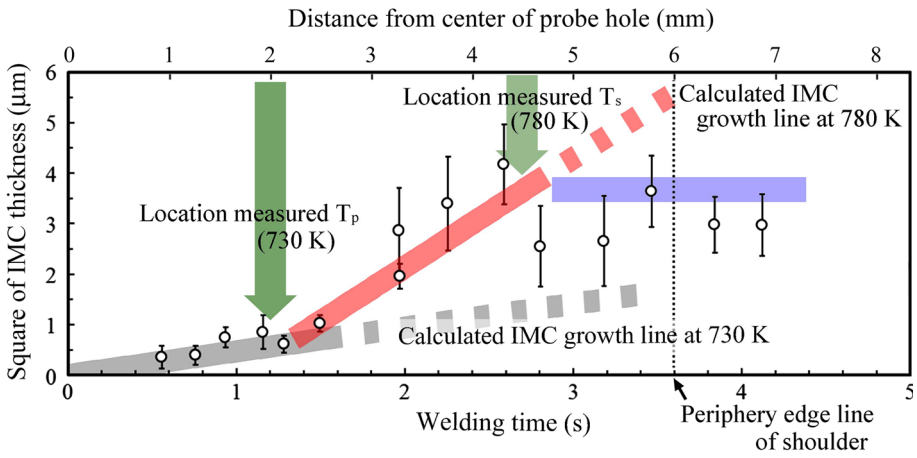

Figure 9 Square of IMC thickness as a function of the heating time and distance from the center of the probe hole.

however, in this study, the calculated IMC growth line is shown in Fig. 9, assuming that the temperature was 780 K. After ~ 1.3 s, the slope of the growth rate was similar to that calculated for a temperature of 780 K (T_s), thus demonstrating that the second growth stage was strongly influenced by the tool shoulder. These findings, which are based on the phenomenon of metallic diffusion, demonstrate that the two rapid growth processes occurred during FSW and were dominated by the contact between the tool probe and shoulder with the metal plates.

In this study, an experimentally obtained IMC growth rate equation during FSW was used in order to verify the existence of two rapid IMC growth processes, but was unable to clarify the IMC growth mechanism or to quantify the growth kinetics during the FSW of aluminum and steel because the temperatures measured experimentally may be inaccurate. It remains very difficult to measure accurate temperatures during FSW because the processed zone is not exposed to the surface and is under isothermal conditions. However, Wang et al. [39] reported that an Fe_2Al_5 layer grew faster than an $FeAl_3$ layer because the diffusion of Fe atoms into Fe_2Al_5 is higher than that of Fe atoms into $FeAl_3$. Additionally, they claimed that the local strain or stress introduced by the welding process contributed to either chemical reactions or interdiffusion because high deformation can provide higher diffusion vacancies and shorter diffusion distances. Therefore, further investigation is needed to clarify the IMC growth mechanism, as well as to quantify the growth kinetics during the FSW of aluminum and steel.

Conclusions

The rapid growth of the IMC during the dissimilar FSW of aluminum alloy and steel was divided into two steps according to the tool contact. Contact between the side of the steel plate and the tool probe caused the temperature to increase, resulting in the first stage of rapid growth. Friction between the tool shoulder and surface of the steel plate also caused a temperature increase that resulted in the second stage of rapid growth. Since the temperature during the second stage was higher than in first, it appears most important to control contact between the tool shoulder and steel plate, along with the plunging pressure, in order to inhibit the growth of IMCs during FSW. Such a strategy could help improve the strength of welds during the fabrication of lightweight materials in the automotive industry. Furthermore, these results could be applied to other dissimilar FSW welds that form IMCs at joint interfaces and thus could be valuable for various industrial applications.

Acknowledgements

We would like to thank Hiroshi Tsuda of Osaka Prefecture University for performing the TEM observations. This work was supported by a Grant-in-Aid for Scientific Research from the Japan Society for the Promotion of Science (Grant Number JP15K18225).

Compliance with ethical standards

Conflict of interest The authors declare that they have no conflict of interest.

References

[1] Schubert E, Klassen M, Zerner I, Wlaz C, Sepold G (2001) Light-weight structures produced by laser beam joining for future applications in automobile and aerospace industry. J Mater Process Technol 115:2–8

[2] Carle D, Blount G (1999) The suitability of aluminium as an alternative material for car bodies. Mater Des 20:267–272

[3] Ishida T (1987) Interfacial phenomena of plasma arc welding of mild steel and aluminium. J Mater Sci 22:1061–1066. https://doi.org/10.1007/BF01103552

[4] Ogura T, Ueda K, Saito Y, Hirose A (2011) Nanoindentation measurement of interfacial reaction layers in 6000 series aluminum alloys and steel dissimilar metal joints with alloying elements. Mater Trans 52:979–984

[5] Sammaiah P, Suresh A, Tagore GRN (2010) Mechanical properties of friction welded 6063 aluminum alloy and austenitic stainless steel. J Mater Sci 45:5512–5521. https://doi.org/10.1007/s10853-010-4609-y

[6] Pardal G, Meco S, Dunn A, Williams S, Ganguly S, Hand DP, Wlodarczyk KL (2017) Laser spot welding of laser textured steel to aluminium. J Mater Process Technol 241:23–35

[7] Lu Y, Mayton E, Song H, Kimchi M, Zhang W (2019) Dissimilar metal joining of aluminum to steel by ultrasonic plus resistance spot welding–Microstructure and mechanical properties. Mater Des 165:10758

[8] Carvalho GHSFL, Galvao I, Mendes R, Leal RM, Loureiro A (2018) Explosive welding of aluminium to stainless steel. J Mater Process Technol 262:340–349

[9] Mori K, Abe Y (2018) A review on mechanical joining of aluminum and high strength steel sheets by plastic deformation. Int J Lightweight Mater Manuf 1:1–11

[10] Thomas WM, Nicholas ED, Needham JD, Murch MG, Temple-Smith P, Dawes CJ (1995) GB Patent Application No. 9125978.8, Dec. 1991; US Patent No. 5460317

[11] Mishra RS, Ma ZY (2005) Friction stir welding and processing. Mater Sci Eng R 50:1–78

[12] Rodriguez NA, Alemanza E, Alvarez CJ (2005) Study of friction stir welded A319 and A413 aluminum casting alloys. J Mater Sci 40:4307–4312. https://doi.org/10.1007/s10853-005-2837-3

[13] Zhang Z, Xiao BL, Ma ZY (2012) Effect of welding parameters on microstructure and mechanical properties of friction stir welded 2219Al-T6 joints. J Mater Sci 47:4075–4086. https://doi.org/10.1007/s10853-012-6261-1

[14] Ji P, Yang Z, Zhang J, Zheng L, Ji V, Klosek V (2015) Residual stress distribution and microstructure in the friction stir weld of 7075 aluminum alloy. J Mater Sci 50:7262–7270. https://doi.org/10.1007/s10853-015-9280-x

[15] Fujii H, Cui L, Tsuji N, Maeda M, Nakata K, Nogi K (2006) Friction stir welding of carbon steels. Mater Sci Eng A 429:50–57

[16] Sato YS, Yamanoi H, Kokawa H, Furuhara T (2007) Microstructural evolution of ultrahigh carbon steel during friction stir welding. Scr Mater 57:557–560

[17] Park SHC, Sato YS, Kokawa H (2003) Microstructural evolution and its effect on Hall–Petch relationship in friction stir welding of thixomolded Mg alloy AZ91D. J Mater Sci 38:4379–4383. https://doi.org/10.1023/A:1026351619636

[18] Xu RZ, Ni DR, Yang Q, Liu CZ, Ma ZY (2015) Influence of Zn interlayer addition on microstructure and mechanical properties of friction stir welded AZ31 Mg alloy. J Mater Sci 50:4160–4173. https://doi.org/10.1007/s10853-015-8841-3

[19] Zhou L, Liu HJ, Liu QW (2010) Effect of process parameters on stir zone microstructure in Ti–6Al–4V friction stir welds. J Mater Sci 45:39–45. https://doi.org/10.1007/s10853-009-3881-1

[20] Mironov S, Sato YS, Kokawa H (2018) Friction-stir welding and processing of Ti–6Al–4V titanium alloy: a review. J Mater Sci Technol 34:58–72

[21] Ye F, Fujii H, Tsumura T, Nakata K (2006) Friction stir welding of Inconel alloy 600. J Mater Sci 41:5376–5379. https://doi.org/10.1007/s10853-006-0169-6

[22] Sato YS, Arkom P, Kokawa H, Nelson TW, Steel RJ (2008) Effect of microstructure on properties of friction stir welded Inconel alloy 600. Mater Sci Eng A 477:250–258

[23] Chen T (2009) Process parameters study on FSW joint of dissimilar metals for aluminum–steel. J Mater Sci 44:2573–2580. https://doi.org/10.1007/s10853-009-3336-8

[24] Ogura T, Saito Y, Nishida T, Nishida H, Yoshida T, Omichi N, Fujimoto M, Hirose A (2012) Partitioning evaluation of mechanical properties and the interfacial microstructure in a friction stir welded aluminum alloy/stainless steel lap joint. Scr Mater 66:531–534

[25] Chen ZW, Yazdanian S, Littlefair G (2013) Effects of tool positioning on joint interface microstructure and fracture strength of friction stir lap Al-to-steel welds. J Mater Sci 48:2624–2634. https://doi.org/10.1007/s10853-012-7056-0

[26] Pourali M, Abdollah-zadeh A, Saeid T, Kargar F (2017) Influence of welding parameters on intermetallic compounds formation in dissimilar steel/aluminum friction stir welds. J Alloys Compd 715:1–8

[27] Hatano R, Ogura T, Matsuda T, Sano T, Hirose A (2018) Relationship between intermetallic compound layer thickness with deviation and interfacial strength for dissimilar joints of aluminum alloy and stainless steel. Mater Sci Eng A 735:361–366

[28] Fukumoto M, Tsubaki M, Shimada Y, Yasui T (2004) Welding between ADC 12 and SS400 by means of friction stirring. J Jpn Weld Soc 22:309–314

[29] Morita T, Sakamoto A, Mabuchi S, Iizuka T (2009) Strength and formability of friction stir welded aluminum alloy with cold rolled steel. J Soc Mater Sci Jpn 58:317–322

[30] Tanaka T, Hirata T, Shinomiya N, Shirakawa N (2015) Analysis of material flow in the sheet forming of friction-stir welds on alloys of mild steel and aluminum. J Mater Process Technol 226:115–124

[31] Kimapong K, Watanabe T (2005) Effect of welding process parameters on mechanical property of FSW lap joint between aluminum alloy and steel. Mater Trans 46:2211–2217

[32] Tanaka T, Morishige T, Hirata T (2009) Comprehensive analysis of joint strength for dissimilar friction stir welds of mild steel to aluminum alloys. Scr Mater 61:756–759

[33] Tanaka T, Morishige T, Hirata T (2011) Formation mechanism of intermetallic compound at the weld interface of dissimilar friction stir welded joint of pure aluminum and mild steel. Q J Jpn Weld Soc 29:101–106

[34] Tanaka K, Kumagai M, Yoshida H (2006) Dissimilar joining of aluminum alloy and steel sheets by friction stir spot welding. J Jpn Inst Light Metal 56:317–322

[35] Sun YF, Fujii H, Takaki N, Okitsu Y (2013) Microstructure and mechanical properties of dissimilar Al alloy/steel joints prepared by a flat spot friction stir welding technique. Mater Des 47:350–357

[36] Van der Rest C, Jacques PJ, Simar A (2014) On the joining of steel and aluminum by means of a new friction melt bonding process. Scr Mater 77:25–28

[37] Movahedi M, Kokabi AH, Reihani SMS, Cheng WJ, Wang CJ (2013) Effect of annealing treatment on joint strength of aluminum/steel friction stir lap weld. Mater Des 44:487–492

[38] Wan L, Huang Y (2018) Friction stir welding of dissimilar aluminum alloys and steels: a review. Int J Adv Manuf Technol 99:1781–1811

[39] Wang T, Sidhar H, Mishra RS, Hovanski Y, Upadhyay P, Carlson B (2019) Evaluation of intermetallic compound layer at aluminum/steel interface joined by friction stir scribe technology. Mater Des 174:107795

[40] Xu L, Robson JD, Wang L, Prangnell PB (2018) The influence of grain structure on intermetallic compound layer growth rates in Fe–Al dissimilar welds. Metal Mater Trans A 49A:515–526

[41] Ogura T, Umeshita H, Saito Y, Hirose A (2009) Characteristics and estimation of interfacial microstructure with additional elements in dissimilar metal joints of aluminum alloys to steel. Q J Jpn Weld Soc 27:174–178

[42] Naoi D, Kajihara M (2007) Growth behavior of Fe_2Al_5 during reactive diffusion between Fe and Al at solid-state temperatures. Mater Sci Eng A 459:375–382